Fermi surface callipering of chromium alloys

1998 J. Phys.: Condens. Matter 10 10375

(http://iopscience.iop.org/0953-8984/10/46/004)

J. Phys.: Condens. Matter **10** (1998) 10375–10382. Printed in the UK PII: S0953-8984(98)97397-0

Fermi surface callipering of chromium alloys

H M Fretwell†, S B Dugdale‡, R J Hughes§, J Brader§, M A Alam§ and A Rodriguez-Gonzalez§

† Department of Physics, MC 273, University of Illinois at Chicago, Chicago, IL 60607, USA
‡ Université de Genève, Départment de Physique de la Matière Condensée, 24 quai Ernest Ansermet, CH-1211 Genève 4, Switzerland
§ H H Wills Physics Laboratory, University of Bristol, Tyndall Avenue, Bristol BS8 1TL, UK

Received 30 April 1998

Abstract. We use maximum entropy to deconvolute the experimental resolution from (projected) 2DACAR (two-dimensional angular correlation of electron–positron annihilation radiation) data for Cr, Mo, V and their alloys. When the original data are subtracted from the deconvoluted data, the difference distribution reveals far more Fermi surface information. It is found that the difference plot may also be used to calliper the N-hole pockets of the projected Fermi surface. The dimensions that we obtain for pure Cr and Mo agree well with those from the literature, although those we obtain for V are smaller. The technique is designed to permit the callipering of the N-hole pocket in certain alloys for eventual comparison with work on oscillatory exchange coupling in magnetic multilayers.

1. Introduction

In this Special Issue, Lathiotakis *et al* [1] present theoretical results obtained from a study of oscillatory magnetic exchange coupling in Fe/Cu-alloy/Fe multilayers and the role of the Fermi surface topology of the non-magnetic spacer layer in determining the period of the oscillatory coupling. The study emphasizes the need for quantitative information on the Fermi surfaces of materials, especially disordered alloys, used in the manufacture of magnetic multilayers. Unfortunately, owing to technical difficulties there is a scarcity of experimental data for these types of disordered alloy. Here we initiate a study of this problem and discuss the potential of 2DACAR (two-dimensional angular correlation of electron–positron annihilation radiation) to calliper the Fermi surface of chromium and its alloys which are widely used as spacer layers. The origin of the exchange coupling in these particular multilayered systems is still controversial.

Chromium has a long history of experimental investigation, due in part to its anti-ferromagnetism at low temperatures ($T_N = 311$ K) and the associated spin-density wave that forms along a single [100] direction in the crystal. The spin-density wave is incommensurate with the lattice and has a period which is inversely proportional to the length of a nesting vector ($Q = (2\pi/a)(1 \pm \delta)$; $\delta = 0.05$) that spans the Γ-centred electron octahedra and H-centred hole octahedra of the paramagnetic Fermi surface (figure 1). Oscillatory magnetostriction and de Haas–van Alphen torque measurements in the antiferromagnetic phase are consistent with a remapped paramagnetic Fermi surface which includes magnetic band gaps along the direction of $\boldsymbol{Q}$ [2]. However, positron annihilation results have

0953-8984/98/4610375+08$19.50

previously indicated little difference between the high-temperature paramagnetic and low-temperature antiferromagnetic phases, perhaps due to residual strain in the sample [3] or more likely due to the difficulties in forming a single-$\boldsymbol{Q}$ domain in the sample.

There are many other potential sites for nesting in the Fermi surface and these may play a crucial role in the long-period oscillatory magnetic behaviour found in magnetic multilayers which contain Cr or Cr-alloy spacer layers [4]. In particular, there is much interest in the short nesting vectors which span the N-hole pockets, electron lenses and electron knobs. The magnitude of these vectors may be accurately determined in good single crystals of Cr using traditional quantum oscillatory techniques like dHvA. But of more interest to us (and the multilayer community) is how these vectors evolve with alloying, and such information is not accessible via traditional techniques. Instead, we hope to show that 2DACAR may be used to probe the Fermi surface of the disordered alloy. We attempt to calliper part of the Fermi surface (the N-hole pocket) from the data. This particular sheet is chosen, as recent theoretical calculations indicate it to be one of the prime candidates for nesting in oscillatory magnetic exchange coupling [5].

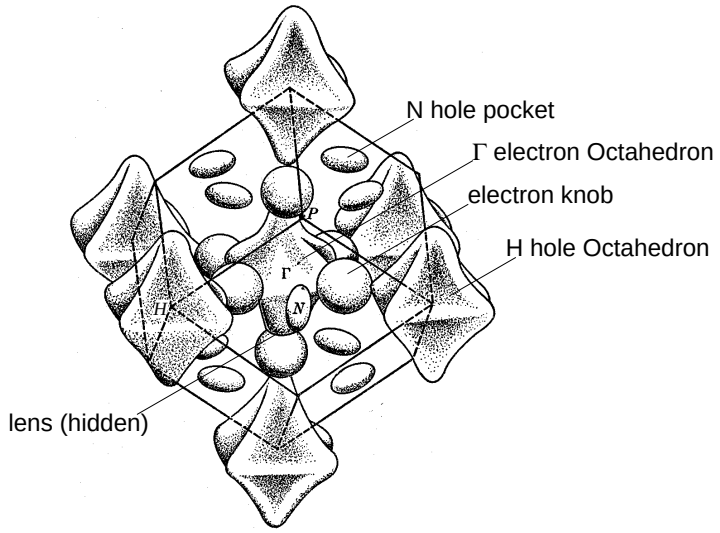

Figure 1. The Fermi surface of Cr showing the Γ-centred electron octahedra, the H-centred hole octahedra, elliptical N-hole pockets, and electron knobs. The electron lenses are hidden in the body of the electron octahedra.

Further, as can be seen from figure 1, in a projection onto a ⟨110⟩ plane, the hole pocket can be quantitatively assessed without resorting to a full three-dimensional reconstruction of the Fermi surface. This consideration is important when one is faced with the need for performing measurements at many different alloy compositions, since individual 2DACAR spectra can take several weeks to accumulate. We use a recently introduced [6] technique based on maximum-entropy deconvolution to calliper the dimensions of the Fermi surface and test its suitability on a model Fermi surface. The technique is then applied to several 2DACAR spectra, measured on different spectrometers under different experimental conditions, to obtain the required callipered dimensions. Finally, we discuss the future direction of the study in terms of improving the callipering technique for its eventual correlation with the observed magnetic multilayer behaviour.

2. Experimental procedure

Our samples originated from several sources and were oriented so that the [110] direction of the crystal lay along the measurement (integration) axis of the spectrometer. We examined the following materials: Cr, $Cr_{0.85}Mo_{0.15}$, Mo, $Cr_{0.95}V_{0.05}$, $Cr_{0.25}V_{0.75}$ and V. For most of the samples, measurements were made at Bristol on a 2DACAR spectrometer with an intrinsic spectrometer angular resolution of 0.57 mrad $\times$ 0.57 mrad (the Brillouin zone dimension (Γ–H) for Cr is $2\pi/a = 8.42$ mrad). The quoted resolution applies only to the spectrometer and does not include thermal contributions or the finite spot size of the positron beam which broadens the resolution parallel to the sample surface (usually aligned along one of the resolved directions). For one sample, $Cr_{0.25}V_{0.75}$, the measurements were made in Geneva at a slightly better resolution [7].

A 2DACAR spectrum represents a projection of the electron–positron momentum density ($\rho^{2\gamma}(\boldsymbol{p})$). In the one-electron approximation, an electron from band j with reduced Bloch wave vector $\boldsymbol{k}$ contributes to $\rho^{2\gamma}(\boldsymbol{p})$ at $\boldsymbol{p} = \bar{h}\boldsymbol{k}$ and also at $\boldsymbol{p} = \bar{h}(\boldsymbol{k} + \boldsymbol{G})$, where $\boldsymbol{G}$ is any reciprocal-lattice vector. The LCW formalism [8] allows us to fold those contributions at finite $\boldsymbol{G}$ back into the first Brillouin zone (where $\boldsymbol{G} = 0$). The resulting LCW distribution represents the projected electron occupation density, $n(\boldsymbol{k})$, in which full bands are transformed to a roughly constant background and Fermi surface 'breaks' are superimposed as steps at $\boldsymbol{k}_F$ (projected steps in the case of 2D data). If the positron wavefunction is independent of $\boldsymbol{k}$, the LCW operation delivers the true electron occupancy in $\boldsymbol{k}$-space; otherwise modulations are introduced into the measurements. In practice, 'positron wavefunction perturbations' are small for simple metals but can be considerable in more complicated electronic structures. In the LCW distribution, these modulations are expected to be slowly varying functions [9], and in our experience they always appear be less sharp, but are occasionally greater in magnitude, than Fermi surface breaks [10]. Fortunately, data analysis techniques have been developed to suppress these problems. The first is known as the 'frequency-limited derivative' technique and is essentially a band-pass filter [9]. The second involves subtracting the original data from the maximum-entropy deconvoluted data (denoted as 'MaxEnt-Raw'). Both techniques act as filters to remove the low-frequency components from the data.

Another factor which affects our ability to determine the Fermi surface is the projected nature of the data. We have shown in the past that very accurate callipering of the Fermi surface can be achieved by reconstructing the three-dimensional Fermi surface from several 2DACAR projections [12]. However, we wish to see here what can be achieved using a single 2DACAR projection. In the past, studies of $Nb_{1-x}Mo_x$ have shown that a second-derivative analysis of the LCW distribution yields a good estimate of the projected N-hole pocket [13]. Taking the derivative is problematic for discrete, noisy data; a small feature such as the N-hole pocket may extend over only 11 channels in the case of our coarsest calibration. Instead, we take a different route and apply maximum-entropy (MaxEnt) deconvolution to the LCW distributions in an attempt to remove the total experimental angular resolution, including thermal contributions. Our FORTRAN program models the resolution as a single Gaussian and uses the Cambridge algorithm [11] and chi-squared statistic to successively iterate towards a solution which best represents the underlying distribution, free from experimental resolution. By using this algorithm it is possible to enhance the Fermi surface breaks (either in 2D or 3D, $\boldsymbol{p}$- or $\boldsymbol{k}$-space) at the expense of relatively smooth, long-range distortions introduced by the positron wavefunction. We then invoke a special property of the MaxEnt-Raw filtering technique to locate the breaks. Taking the difference between an enhanced and raw spectrum removes all long-range distortions, so

reducing the positron wavefunction perturbations and leaving sharper Fermi surface features. As MaxEnt deconvolution is an 'honest' method, which should not shift the position of the Fermi breaks, their positions will be marked by zero-crossings at $\boldsymbol{k}_F$ in the difference spectrum. Therefore the zero contour in the difference plot should reveal the Fermi surface. This idea is strictly valid only in 3D where the steps are sharp. In a 2DACAR distribution, the sharp discontinuities are smeared by projection and from overlap with other sheets. It is the validity of our callipering technique in 2D, given these factors, which we need to check using a model Fermi surface.

The width of the resolution used during deconvolution is both sample and experiment dependent, but we found that the actual width had little bearing on the Fermi surface dimensions obtained in the MaxEnt-Raw callipering technique.

3. Results

To test the MaxEnt-Raw method we generated model Fermi surfaces for Cr, Mo and V with an N-hole pocket size chosen in accordance with previous estimates [14–17]. This

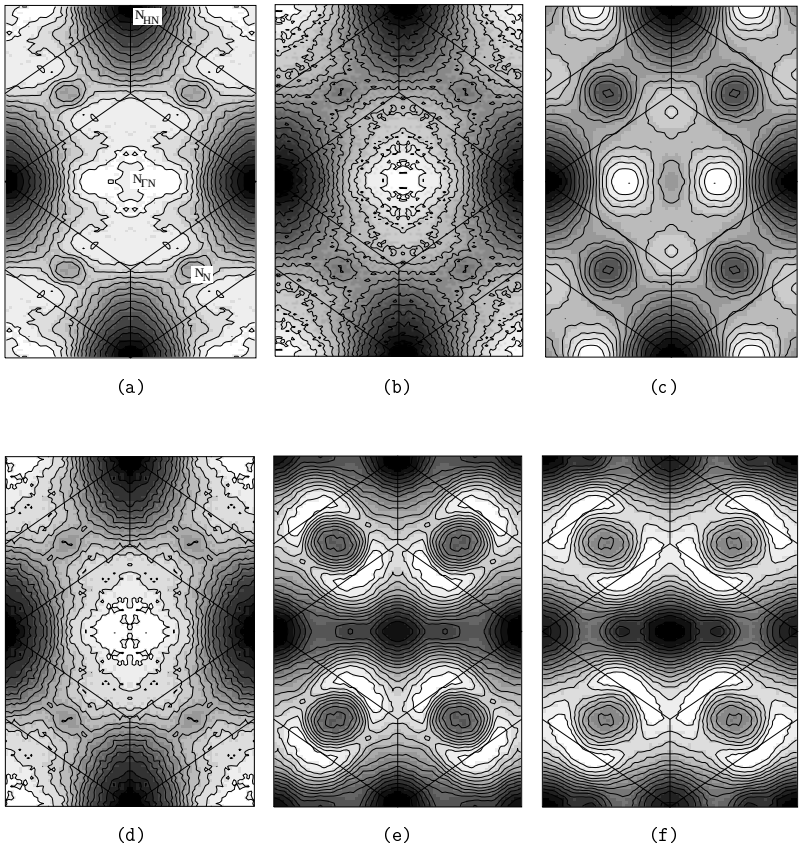

Figure 2. [110] LCW distributions for (a) Cr, (b) $Cr_{0.85}Mo_{0.15}$, (c) Mo, (d) $Cr_{0.95}V_{0.05}$, (e) $Cr_{0.25}V_{0.75}$, (f) V. The resolved directions are $x = [110]$, $y = [100]$ and a projected Brillouin zone is drawn in each figure for clarity. Electron sheets appear as light areas and holes as dark areas. The N-hole pocket that we chose to calliper is located at N_N.

model is projected down the [110] direction (the experimental integration direction) and the MaxEnt-Raw method applied. It was apparent once we began that the only sheets which could be correctly callipered in the [110] direction were the N-hole pockets. All other sheets, such as the electron lens and electron knobs, gave incorrect callipered dimensions due to overlap from other sheets. But as can be seen in figure 1, the four N-hole pockets above (and four below) the central plane are cleanly projected along the [110] direction.

From the model, we found the method correctly assessed the size of the N-hole pockets in Mo and V, but slightly overestimated (by ∼2%) smaller pockets equivalent to those found in Cr. It should be pointed out that the N-hole pockets were modelled as spheres, and not ellipsoids as expected from other work [14–17]. Thus any callipered dimension obtained from a [110] projection can be compared directly with the input radius. In the case of the experiment, the hole pocket is an ellipsoid whose orientation must be taken into account when comparing our experimentally derived dimensions with previous estimates of the major- and minor-axis dimensions along NP, NΓ and NH. Another limitation of the model is the absence of any positron-induced perturbations, but we hope to rectify this in the future. Despite these limitations, the agreement that we find is gratifying and it gives us some confidence in our ability to calliper the N-hole pockets.

We now turn to the experimental data. Figure 2 shows the LCW folded 2DACAR data

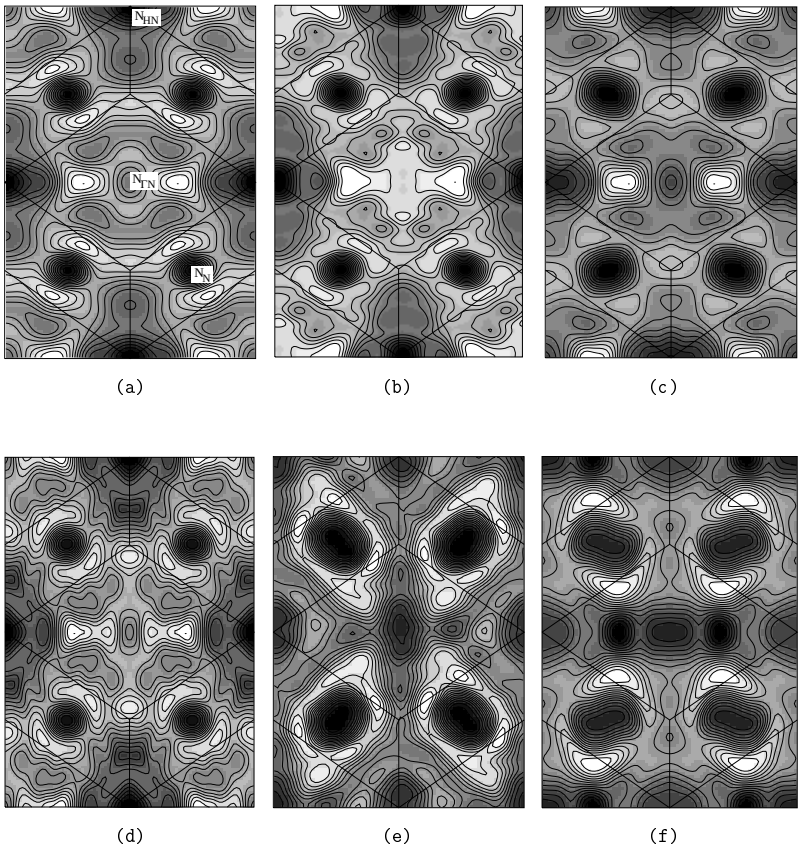

Figure 3. The MaxEnt-Raw difference for the materials listed in figure 2. Note the more pronounced N_N pockets for Cr.

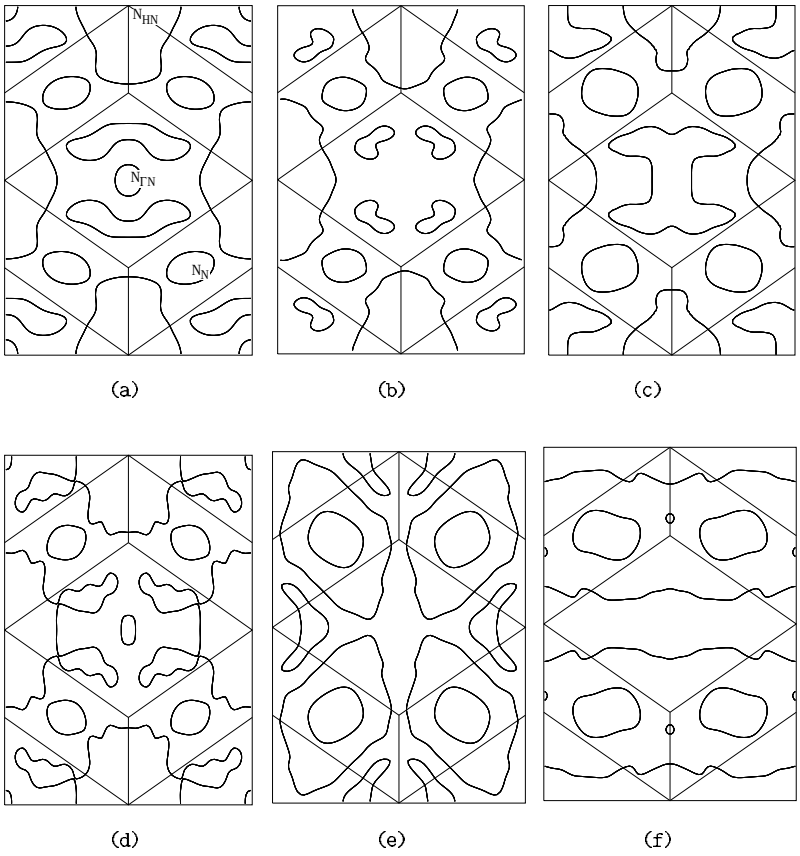

Figure 4. The zero contour in the MaxEnt-Raw difference. The outlines of the projected N_N pockets are clearly visible.

for all of the materials studied. Note the much larger N-hole pockets (at N_N) in Mo and V and their near absence in Cr. It is apparent from the figures that the disordered alloys have a well defined Fermi surface and there is a steady evolution in the raw data as a function of concentration. We have suggested in the past [18] that the N-hole pockets in Cr (which are smaller than those in Mo) may be obscured in the LCW picture by the positron wavefunction perturbations and that one way to remove these is via the MaxEnt-Raw technique which filters out the low-frequency components in the data. The application of this technique gives the 'difference' distributions presented in figure 3. It should be noted that the use of the band-pass technique [9] yields similar pictures. The N-hole pockets for Cr are now more pronounced and there is a clear increase in size as the V or Mo content increases in the alloy samples. In figure 4 we plot the zero contour from the difference which reveals the outline of the projected N-hole pockets. To estimate the size of the N-hole pocket, a vertical slice is taken through the centre of the N_N pocket and the distance between the zero-crossing points is measured. This particular direction is chosen as it is closest to the [110] N–H direction, a commonly used growth direction in magnetic multilayer systems. Unfortunately, it is not possible to obtain this measurement directly from the width of the central N pocket as it projects onto other (electron) sheets at Γ; see figure 1. At this stage we only have an approximate value for the hole dimension as we are looking at the projection

down a direction which lies at an angle to the main ellipsoid axes. Work is in progress in an attempt to derive the main ellipsoid axis dimensions by analysing the shape of the zero contour in the difference plot and comparing with the projected outline of ellipsoids derived from recent KKR-CPA calculations for the elements and their alloys [5].

Table 1. Diameters of the N-hole pockets for Cr, Mo and V. The present work corresponds to a projected diameter (see the text) and previous estimates are along the major and minor axes of the ellipsoid. All of the values are in units of $2\pi/a$. To convert to Å^{-1}, multiply by $2\pi/a$.

Element	Present work	Previous estimates			Lattice parameter a (Å)
		NH	NΓ	NP	
Cr	0.182 ±0.002	0.158 [14, 15] 0.210 [14, 15]	0.215 [14, 15] 0.340 [14, 15]	0.246 [14, 15] 0.344 [14, 15]	2.88
Mo	0.266 ±0.002	0.2168 [16]	0.3248 [16]	0.3616 [16]	3.15
V	0.260 ±0.002	0.3508 [17]	0.4235 [17]	0.4453 [17]	3.02

Our estimates of the (projected) callipered dimension for Cr, V and Mo (averaged over various dimensions due to the projection) are shown in table 1 together with those for the individual dimensions of the N ellipsoids found in the literature. The error that we quote reflects the accuracy with which we can determine the dimension from the difference plot and does not take into account other systematic errors—for example, sample misalignment (<1–2°). We should also point out that the room temperature lattice parameter has been used to calculate the projected reciprocal-lattice vectors (for LCW folding) yet each material was measured at low temperature. Fortunately, the thermal expansion of these materials is small over the temperature range in question, but a thermally induced change in the lattice parameter may have a small effect on the calculated LCW distribution. Our estimates for the size of the projected N-hole pocket for Cr and Mo lie between the NH and NΓ values quoted from other work (which they should, given the [110] projection). However, our callipered dimension for V is slightly smaller than those quoted. A second-derivative analysis of the vanadium N-hole pocket in the LCW distribution yielded a very similar result to the present MaxEnt-Raw technique. We suggest that as the alloys approach V, the N-hole pocket becomes so large that it overlaps with surrounding Fermi surface sheets, so distorting its apparent size. This view is consistent with the larger N-hole pocket that we find in $Cr_{0.25}V_{0.75}$ where there is less problem from overlap. Exactly why such an effect is not seen in the model, where similar large N-hole dimensions were used, is still under investigation. We suggest that a full 3D reconstruction may be necessary for the V-rich $Cr_{1-x}V_x$ alloys.

4. Conclusion

We have shown that it is possible to derive reliable dimensions for the N-hole pocket in Cr, Mo and their alloys from (projected) 2DACAR data without the need for 3D reconstruction of the Fermi surface. More work is needed to get the three main axes of the N-hole pocket and this is currently in progress.

For V-rich $Cr_{1-x}V_x$ alloys the situation looks problematic. The dimensions that we obtain from 2DACAR are smaller than those derived from theory and other experiments. Our simple model analysis suggests that it should be possible to measure the N pocket in

V, but we speculate that the discrepancy arises from an overlap with other sheets in the 2D data.

It is believed that a vector spanning the N-hole pocket is a prime candidate for driving the oscillatory magnetic exchange coupling found in the magnetic multilayers. The technique that we present here can potentially be used to identify all possible nesting vectors in $Cr_{1-x}Mo_x$ and dilute $Cr_{1-x}V_x$, and monitor their evolution (as a function of material or alloy concentration) for comparison with the multilayer behaviour.

Acknowledgments

We are indebted to Alfred Manuel for allowing us to use his unpublished data on $Cr_{0.25}V_{0.75}$. This work was supported by the EPSRC (UK), the Royal Society and the Swiss National Fund.

References

[1] Lathiotakis N, Gyorffy B and Staunton J 1998 *J. Phys.: Condens. Matter* **10** 10 357
[2] Fawcett E, Griessen R and Stanley D J 1976 *J. Low Temp. Phys.* **25** 771
[3] Bull C R, Alam A, Shiotani N, West R N, Singru R M and Singh A K 1986 *Positron Annihilation* ed P C Jain *et al* (Singapore: World Scientific) p 266
[4] Parkin S S P, More N and Roche K P 1990 *Phys. Rev. Lett.* **64** 2304
Parkin S S P 1993 *Bull. Am. Phys. Soc.* **38** 561 (abstract)
van Schilfgaarde M, Herman F, Parkin S S P and Kudrnovsky J 1995 *Phys. Rev. Lett.* **74** 4063
[5] Stiles M D 1996 *Phys. Rev.* B **54** 14 679
Tsetseris L, Lee Byungchan and Chang Yia-Chung 1997 *Phys. Rev.* B **55** 11 586
[6] Dugdale S B 1995 *PhD Thesis* University of Bristol
[7] For a description of the spectrometer, see
Vasumathi D, Barbellini B, Manuel A A, Hoffman L and Jarlborg T 1997 *Phys. Rev.* B **55** 11 714
[8] Lock D G, Crisp V H C and West R N 1973 *J. Phys. F: Met. Phys.* **3** 561
[9] O'Brien K M, Brand M Z, Rayner S and West R N 1995 *J. Phys.: Condens. Matter* **7** 925
[10] Biasini M, Alam M A, Harima H, Onuki Y, Fretwell H M and West R N 1994 *J. Phys.: Condens. Matter* **6** 7823
[11] Skilling J and Gull S F 1985 *Algorithms and Applications; Maximum-Entropy and Bayesian Methods in Inverse Problems* ed C R Smith and W T Grandy Jr (New York: Reidel) pp 83–132
[12] Dugdale S B, Fretwell H M, Alam M A, Kontrym-Sznajd G, West R N and Badrzadeh S 1997 *Phys. Rev. Lett.* **79** 941
[13] Kaiser J H, Walters P A, Bull C R, Alam A, West R N and Shiotani N 1987 *J. Phys. F: Met. Phys.* **17** 1243
Bull C R, Kaiser J H, Alam A, Shiotani N and West R N 1984 *Phys. Rev.* B **29** 6378
[14] Rath J and Calaway J 1973 *Phys. Rev.* B **8** 5398
[15] Graebner J E and Marcus J A 1968 *Phys. Rev.* B **175** 659
[16] Ketterson J B, Koelling D D, Shaw J C and Windmiller L R 1975 *Phys. Rev.* B **11** 1447
[17] Parker R D and Holloran M H 1974 *Phys. Rev.* B **9** 4130
[18] Fretwell H M, Rodriguez-Gonzalez A, Dugdale S B, Alam M A, Singru R M, Sundararajan V, Cooper M and Shiotani N 1997 *Mater. Sci. Forum* **255–257** 417
and see also
Dugdale S B, Fretwell H M, Hedley D C R, Alam M A, Jarlborg T, Santi G, Singru R M, Sundararajan V and Cooper M J 1998 *J. Phys.: Condens. Matter* **10**